Near-infared hyperspectral imaging of teeth for dental caries detection

Christian Zakian
Iain Pretty
Roger Ellwood
The University of Manchester
Dental Health Unit
School of Dentistry
Oxford Road
Manchester, M13 9PL
United Kingdom

Abstract. Near-infrared (NIR) is preferred for caries detection compared to visible light imaging because it exhibits low absorption by stain and deeper penetration into teeth. Hyperspectral images from 1000 to 2500 nm have been obtained for a total of 12 extracted teeth (premolars and molars) with different degrees of natural lesion. Analysis of the reflectance spectra suggests that light scattering by porous enamel and absorption by water in dentin can be used to quantify the lesion severity and generate a NIR caries score. Teeth were ground for histological examination after the measurements. The NIR caries score obtained correlates significantly (Spearman's correlation of 0.89, $p < 0.01$) with the corresponding histological score. Results yield a sensitivity of >99% and a specificity of 87.5% for enamel lesions and a sensitivity of 80% and a specificity >99% for dentine lesions. The nature of the technique offers significant advantages, including the ability to map the lesion distribution rather than obtaining single-point measurements, it is also noninvasive, noncontact, and stain insensitive. These results suggest that NIR spectral imaging is a potential clinical technique for quantitative caries diagnosis and can determine the presence of occlusal enamel and dentin lesions. © *2009 Society of Photo-Optical Instrumentation Engineers.* [DOI: 10.1117/1.3275480]

Keywords: biomedical optics; medical imaging; spectroscopy; image processing; image segmentation; infrared imaging.

Paper 09255R received Jun. 18, 2009; revised manuscript received Nov. 2, 2009; accepted for publication Nov. 4, 2009; published online Dec. 29, 2009.

1 Introduction

Dental caries is a dynamic disease characterized by tooth demineralization leading to an increase in the porosity of the enamel surface—commonly known as white spots due to the white appearance created by the increased refractive index gradient.[1] Leaving these lesions untreated can potentially lead to cavities reaching the dentin and pulp and eventually causing tooth loss. Occlusal and approximal surfaces are among the most susceptible sites of demineralization due the acid attack from bacterial by-products in the biofilm.[2] The use of preventive agents to inhibit, or reverse the demineralization process is predicated on the detection of lesions at an early stage.[3–6] However, detecting early lesions is a difficult diagnostic task and quantitative techniques are still required particularly to monitor the caries lesion progression or arrest and therefore to assist in the decision making.

Noninvasive detection of white spots relies on the estimation of surface porosity or mineral loss. Although radiographic methods are suitable for approximal surface lesion detection, they offer a reduced utility for screening early caries in occlusal surfaces due to their lack of sensitivity at very early stages of the disease.[7–9] Electrical caries monitoring has demonstrated good performance for single-point measurements;[10,11] however, imaging methods have the advantage of being more illustrative and allow relative measurements between different sites in the same tooth. Optical methods have been exploited due to their nondestructive nature and ability to detect early demineralization.[12,13]

New potential methods include polarized Raman spectroscopy,[14] multiphoton imaging, infrared tomography, infrared fluorescence, optical coherence tomography (OCT), and terahertz imaging.[15] Current imaging methods are based on the observation of the changes of the light transport within the tooth, namely absorption, scattering and/or fluorescence of light. Porous media scatters light more than uniform media and stain tends to absorb the light. Fiber-optic transillumination (FOTI) is a qualitative method used to highlight the lesions within teeth by observing the patterns formed when white light, pumped from one side of the tooth, is scattered away and/or absorbed by the lesion.[16] DiFOTI™ is a digital technique that is based on the transillumination of light through teeth for the assessment of dental caries.[17] This technique is however difficult to quantify due to an uneven light distribution inside the tooth. This drawback is partially overcome with quantitative light fluorescence (QLF), an imaging method that relies on the natural fluorescence of teeth.[18,19] This fluorescence acts as an internal source of light that will try to escape through the surface of the tooth. With appropriate filters, one can observe the fluorescent light and can quan-

Address all corresponding to: Christian Zakian, The University of Manchester, Dental Health Unit, School of Dentistry, Oxford Road, Manchester, M13 9PL, United Kingdom. Tel: 44-0-16-12261211; Fax: 44-0-16-12324700; E-mail: christian.zakian@manchester.ac.uk.

tify the loss of mineral by visualizing the dark patches produced by scattering and/or absorption of light. QLF is a promising technique; however it has a downfall when trying to discriminate between white spots and stain because both produce the similar effect (extinction of light shadows). Stain is commonly observed in the occlusal sites of the teeth, and this obscures the true detection of caries. Stain therefore is one of the most crucial confounding factors in the detection of early caries lesions.

It has been shown however that working in the near-infrared (NIR) region of the spectrum can overcome the difficulties found with the imaging methods because scattering in enamel is reduced and absorption by stain is low.[20–24] In fact, it has been demonstrated that the scattering by enamel tissues reduces in the form of $1/\lambda^3$ as reported for laser wavelengths, λ, of 512, 632, and 1053 nm.[20] In addition, a higher transparency for 1310 nm than for 1550 nm in sound enamel has been found, suggesting that water in the enamel attenuates the light at higher wavelengths.[21] This has been used in optical coherence tomography for structural imaging of teeth and in tooth transillumination for interproximal and occlusal caries screening.[25] It has been demonstrated that stimulated lesions in tooth samples up to 6.75 mm in thickness can be resolved with a contrast ratio of >0.35 between sound and demineralized enamel by using 1310 nm.[22] Although NIR imaging has shown a potential for delimiting carious regions successfully, not much work has been done to quantify the degree of lesions in naturally decayed teeth.

Our aim is to show for the first time that spectral imaging in the NIR region could be used to map and quantify the lesions from occlusal tooth surfaces by using the spectral signatures of water absorption and the effect of porosity in the scattering of light.

2 Materials and Methods

2.1 Sample Preparation

Twelve extracted human teeth (premolars and molars) with natural lesions of various degrees were acquired from the Oral Health Centre of the University of Indiana, USA. At this facility, soft tissues were removed from the collected teeth and these were thoroughly cleaned. Each tooth was stored in a separate container with distilled water and 0.5% thymol to keep them hydrated and sterile and therefore free from bacteria before imaging. The excess of water on the occlusal surfaces was however gently wiped off using a cotton.

2.2 Instrumentation

An NIR hyperspectral camera system (Spectral Camera SWIR, ImSpector, Finland) was used to capture the spectral reflectance from the samples. The instrument images a line of vision at a time and diffracts the light onto a two-dimensional mercury cadmium tellaride (MCT) sensor array using a diffraction grating. A complete stack of spectral images (spectral data cube) is obtained by translating the sample at constant speed and line-imaging synchronously. The spectral analysis range was from 1000 to 2500 nm with a spectral resolution of 10 nm. Figure 1 shows an image of the system setup. Note that a two-side illumination using halogen lamps was configured to reduce the shadowing effects.
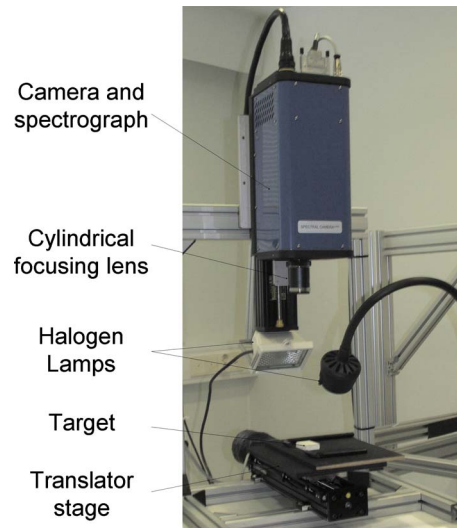

Fig. 1 NIR hyperspectral imaging system. For our investigations, the targets were teeth having different degrees of lesion.

Calibrated spectral reflectance data were obtained using the system's associated software (ENVI 4.3 + in-build ImSpector add-ons). The calculation required to input a "raw" spectral data cube file, a dark current measurement associated with the data acquired (for noise subtraction), the reflectance spectra of a reference object, and its associated dark current measurement. The following calculation was performed for each pixel:

$$R(\lambda) = \frac{R_{\mathrm{r}}(\lambda) - D_{\mathrm{r}}}{W_{\mathrm{ref}}(\lambda) - D_{\mathrm{w}}} W_{\mathrm{spec}}(\lambda). \qquad (1)$$

Here $R(\lambda)$, $R_{\mathrm{r}}(\lambda)$, and $W_{\mathrm{ref}}(\lambda)$ are the calibrated, raw and white reference measurements at wavelength λ, respectively. $W_{\mathrm{spec}}(\lambda)$ corresponds to the white reference reflectance at wavelength λ as specified by the manufacturer. In addition, D_{r} and D_{w} are the dark current noise measurements obtained for the raw and white reference reflectance data.

2.3 Histology

Serial histological sectioning was used as the gold standard to validate the NIR hyperspectral measurements. Teeth were mounted in acrylic resin blocks and submillimeter grounding steps of 0.1–2 mm were performed along the transversal plane to their surface. Photographs were taken after each step, repositioning the block at the same distance to the camera to keep constant illumination. A representative slice was selected for each tooth and scored to agreement by a panel of two expert dentists to ensure reliability. The score was based on the criteria shown in Table 1. Note that the score was given by looking at the deepest lesion observed on the slice.

2.4 Image Analysis

As an example, a selection of the spectral images obtained from an occlusal tooth surface is shown in Fig. 2 at the wavelengths indicated. It is possible to see that the reflectance intensity drops at higher wavelengths. A typical reflectance spectrum for sound, white-spot (enamel lesion), and a dentin

Table 1 Histology scoring criteria.

Score	Lesion depth
S	Sound (no lesion)
E1	1/3 enamel
E2	2/3 enamel
EDJ	Enamel-dentin junction
D1	1/3 dentin
D2	2/3 dentin
D3	To the pulp

Fig. 3 Example of NIR spectral reflectance curves from an occlusal tooth surface. The example shows the reflectance for a sound (black ♦), an enamel lesion (blue ∗), and a dentin lesion (red ○) region. The inset picture shows the location of the points selected within the tooth for this example. Vertical dotted lines indicate the wavelengths chosen for the example in Fig. 2. (Color online only.)

lesion areas is shown in Fig. 3. Well-defined signatures can be observed among the three cases. For instance, the reflectance above 1400 nm is clearly higher for the decayed areas and, in particular, at 1610 nm. However, the absorption dips are further pronounced for the case of dentin lesion and especially at 1440 nm.

The spectral intensity at each pixel was normalized to the reflectance obtained at 1090 nm because it is the wavelength with the highest reflectance (least extinction). The degree of enamel, S_e, and dentin, S_d, lesions were therefore calculated as follows:

$$S_e = \frac{R(1610 \text{ nm})}{R(1090 \text{ nm})}, \qquad (2)$$

$$S_d = \frac{R(1610 \text{ nm}) - R(1440 \text{ nm})}{R(1090 \text{ nm})}. \qquad (3)$$

A caries score, S_{caries}, was calculated as a combination of S_e and S_d and was designed to account for the deepest lesion observed by the NIR spectrum as follows:

$$S_{caries} = p\left(\frac{S_e - K_e}{N_e}\right) + (1-p)\left(1 + \frac{S_d - K_d}{N_d}\right). \qquad (4)$$

Here, K_x and N_x are the enamel (x:e) and dentin (x:d) score calibration offset and normalization factor, respectively. In addition, $p=1$ if $[1+(S_d-K_d)/N_d] < S_{dth}$, where S_{dth} represents the dentin lesion threshold, otherwise $p=0$. Note that S_{caries} depends on either but not both scores simultaneously. S_e is linked to the enamel scattering through the spectral signature sitting around 1610 nm, whereas S_d is linked to the water absorption normally in carious dentin through spectral signature sitting around 1440 nm; the strongest effect is the one accounted for by S_{caries}.

Outliers and noise introduced by specular reflections were removed by limiting the values of the numerators in Eq. (4) to the range $0 < (S_e - K_e) < M_e$ and $0 < (S_d - K_d) < M_d$; here M_e and M_d denote the upper limits. Values outside these limits were set to zero.

To fix the range of S_{caries} from 0 to 2, the normalization factors in Eq. (4) were expressed as $N_e = M_e / S_{dth}$ and $N_d = M_d$. Therefore, for values in the range of $S_{eth} < S_{caries} \leq S_{dth}$, where S_{eth} represents the enamel lesion threshold, the score indicates an enamel lesion and for $S_{caries} > S_{dth}$, the score indicates a dentin lesion. Note that sound areas have a value of $S_{caries} \leq S_{eth}$.

The calibration values for the equations above were obtained empirically. For our case, results were best described with $S_{dth}=0.05$, $S_{dth}=1.1$, $K_e=0.14$, $K_d=0.05$, $M_e=0.35$, and $M_e=0.15$.
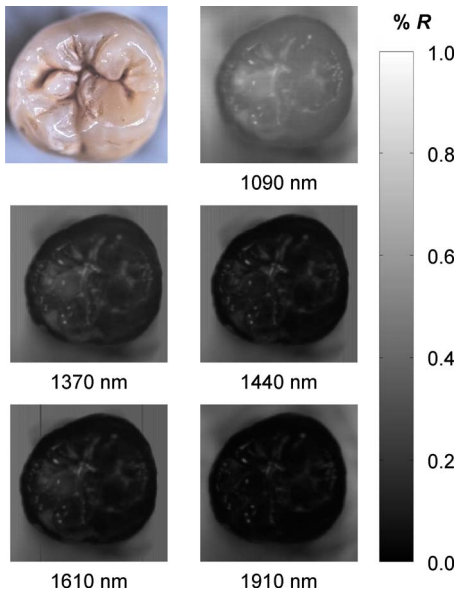

Fig. 2 Selection of spectral images. On the top left, a color picture of the tooth is shown. The remaining reflectance images are obtained with the NIR hyperspectral camera at the wavelengths indicated. (Color online only.)
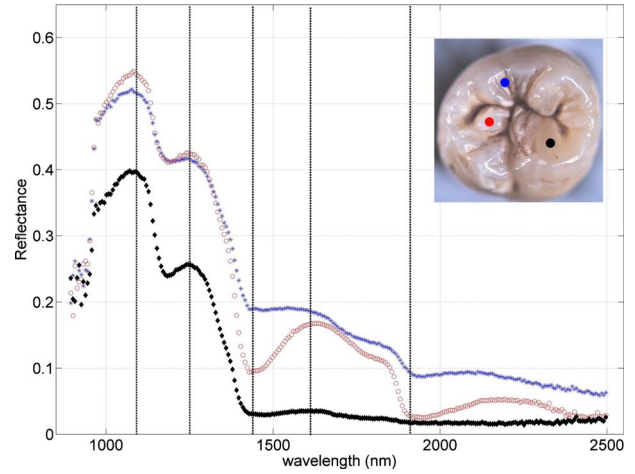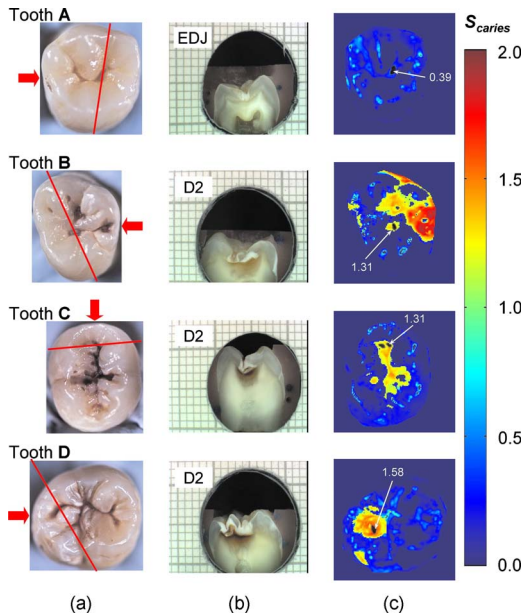
Fig. 4 Examples of teeth with different carious lesions. (a) Images show the color picture for each tooth, (b) Images show the corresponding histological section indicated by the red line in the color picture with the red arrow indicating the point of view of the section. (c) Images show the false-color NIR caries maps, spatially scored using S_{caries}, for each tooth. (Color online only.)

Fig. 5 Sample distribution according to their histology score.

2.5 Statistical Analysis

A region from each of the S_{caries} maps corresponding to the selected histological section was obtained. A histogram of the values obtained across this region was calculated, and the value corresponding to the highest bin with more than five pixels was extracted. This removes false maxima that could be caused by specular reflections. The average of the values within the extracted bin was used as an indication of the maximum S_{caries} score in the region and was compared to the histology score.

3 Results

Twelve teeth with different lesion degrees were imaged and processed following the method described in Section 2.5. As an example, false-color-coded S_{caries} maps for four teeth are shown in Fig. 4. The associated color pictures and the selected histological sections chosen are also shown.

Note that the extension of the lesion is not evident from the color pictures (which rely on visible wavelengths). It is possible to see however that the caries score maps clearly depict the lesion spatial distribution. This is possible due to the longer light penetration of NIR wavelengths through enamel. In addition, the depth of the lesions can be confirmed from the histological sections. The red arrows pointing toward the color picture indicate the point of view of the histological section, which is indicated by the red line.

For the examples presented in Fig. 4, lesion in tooth A rest within the enamel, having $S_{caries} < 1.1$, whereas the lesions in teeth B, C, and D reach the dentin, having $S_{caries} > 1.1$. This observations can be confirmed with the histological sections shown and scored as EDJ for tooth A and D2 for teeth B, C,

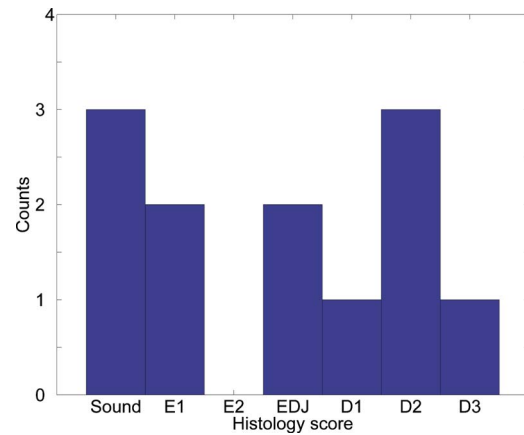and D. The black points highlighted in each image correspond to the maximum scores found within the region corresponding to the histological section and the average value is indicated by the arrow.

Hidden lesions as the one in tooth D are of particular interest since visual inspection does not reveal them easily and they could be left untreated increasing the risk of tooth loss. It is clear from the histology section that the damage has reached the dentin for this case and this is adequately indicated by values of $S_{caries} > 1.1$ around the decayed region.

Detection of caries in pits and fissures is of great interest among the dental practitioners because demineralization commonly starts in these sites and the detection of them is not always obvious, especially in the presence of stain. The decay in the fissure pattern of tooth A can be easily discriminated in the S_{caries} map; the demineralized part of the U-shaped fissure of this tooth is well described and confirmed with the histological section. Enamel demineralization in the fissure pattern of the remaining teeth shown in Fig. 4 are also depicted by their corresponding S_{caries} map, but the deepest tooth lesion is the one considered for our statistical analysis below.

Areas in which there has been complete loss of tooth tissue creating a cavity (i.e. a hole), as the ones appearing in the right side of teeth B and C, yield low values for S_{caries}. We believe this is caused by insufficient mineral and water to create a significant change in the spectrum. More investigations are needed to see the effects of exposed dentin when scoring the tooth with this method.

The NIR images are affected by specular reflection and particularly around the edges and the crests of the teeth, where reflections are expected to be strong. These reflections act as a noise factor, especially for the calculation of S_e in Eq. (2). Note that the stain and pigmentation in all teeth did not show a significant interference with the measurements.

It is important to emphasize that a direct relationship between histological depth and the magnitude of S_{caries} has yet to be determined; however, it can be seen that the NIR algorithm discriminates well between sound, enamel, and dentin lesions.

A histogram showing the distribution of samples according to the different histological scores is shown in Fig. 5. Note that three selected samples had a representative histological
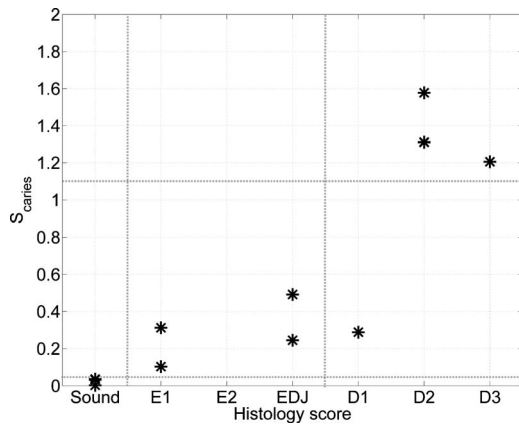
Fig. 6 Correlation plot of the histological score and the average maximum NIR caries score, S_{caries}, within the map region corresponding to the histological section.
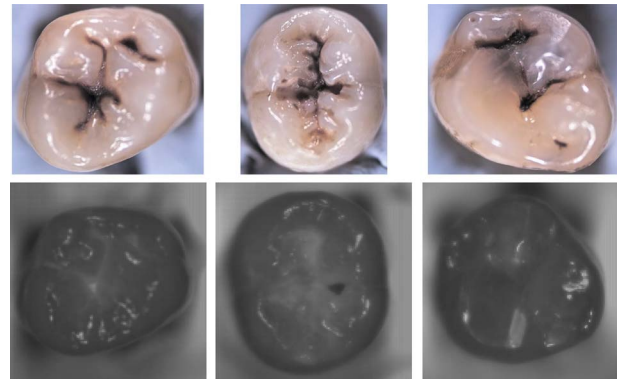

Fig. 7 NIR images of highly stained occlusal tooth surfaces taken at 1250 nm. It can be clearly observed that the absorption by stain is minimal and shows little influence to reveal underlying tooth decay.

sound slice, four had a slice with an enamel lesion, and five had a slice with a dentin lesion.

Figure 6 shows a correlation graph between the two scores and a Spearman's correlation 0.89 significant at a level $p < 0.01$ was found. In addition, a sensitivity of $>99\%$ and a specificity of 87.5% for enamel lesions and a sensitivity of 80% and a specificity $>99\%$ for dentine lesions were found using the NIR spectral imaging method.

4 Discussion

There is great interest to detect early stages of tooth decay because it is reversible, and the progression to a stage where restorative intervention is required can therefore be avoided. Screening early lesions in occlusal pits and fissures is a main concern because these regions have a higher susceptibility to bacterial deposition and therefore demineralization. Radiography and visual inspection are commonly used in the clinic to perform this task; however, the former method lacks the sensitivity needed to detect early stages of the disease and both lack the ability to quantify its progression successfully. Although FOTI has been used to improve the detection of caries in occlusal and interproximal surfaces,[9,16] quantification is still an issue and the excess of light scattering and therefore reduced penetration in visible wavelengths (400–700 nm) imposes a performance limitation. Moreover, stain is a strong confounding factor that affects this technique.

The most promising quantitative methods for occlusal caries detection previously reported include QLF,[26] laser red fluorescence,[27] and ECM.[10] Although OCT is still in an experimentally stage, it has also shown the ability to examine tooth structure non-invasively.[25,28] The downfall of electrical caries monitoring is that it is a single-point measurement and not much information about the lesion distribution can be obtained. Laser red fluorescence is also single-point technique and is mainly designed to detect bacterial invasion, but a strong fluorescence signal is normally obtained only when the lesion is already in the dentin. QLF is mainly designed for the detection of enamel lesions; however, stains represent a strong confounding factor for this technique. Bühler et al.[29] have recently introduced NIR imaging as a method for occlusal caries detection. This method operates in the same manner as

FOTI but employs NIR wavelengths and therefore improves the light penetration through the enamel, increases the image contrast, and can reveal the presence of hidden lesions. The technique was therefore proposed by the authors for delineating the lesions and possibly used in combination with OCT. Although excellent results are reported with NIR imaging, quantification of the lesions is difficult when employing a transillumination configuration due to the shadows created within the samples and the image bleaching caused by the side illumination. An improved uniform illumination was however obtained by using a cylindrical collimating lens.[29] These results are nevertheless encouraging, but only wavelengths of 830,[30] 1310, and 1550 nm (Refs. 21 and 29) have been explored in the NIR for caries detection.

Hyperspectral imaging is a powerful method used to interrogate the spectral characteristics of samples in a two-dimensional space. This feature is of particular use when studying teeth due to their inherent heterogeneous occlusal geometry and associated lesion distribution. We have employed this method for our investigations to demonstrate the ability of NIR spectral imaging to quantify caries lesions from occlusal surfaces. Note that we have used a reflectance configuration since uniform illumination of the tooth is easily achieved. Imaging with NIR wavelengths is of great interest since stain no longer represents a strong confounding factor when detecting tooth demineralization. Figure 7 shows an example of the reflectance obtained at a wavelength of 1250 nm for three heavily stained teeth. It is possible to observe that the absorption of light by stain is minimal and confirms previous reported observations employing NIR wavelengths.[29]

Note that the spectral intensity dips observed in the reflectance spectra shown in Fig. 3 correspond to the absorption peaks of water. In addition, the expected raise in light scattering caused by white spot lesions can be observed in the spectra as a background intensity across all wavelengths. The results obtained for the different lesions suggest that, as the cavity reaches the dentin, the lesion size increases and the amount of water within also increases. For early enamel demineralization, the effect is rather observed as an augmented light scattered intensity at the surface due to the porous structure of the lesion. These physical effects are used as a mechanism to quantify the extension of tooth decay; in particular we proposed to use the reflectance at 1440 and 1610 nm as pre-

sented in Eq. (4) since these wavelengths prove to be most affected by water absorption and scattering, as shown in Fig. 3, for enamel and dentin lesions. Sound regions of the teeth show a reduced reflectance at wavelengths above 1450 nm; this might be caused by an increase in the absorption of light by hydroxyapatite and/or collagen; decayed areas have a reduced amount of mineral and/or organic material, and this can explain the observed higher reflectance at such wavelengths.

Although special attention was paid to remove the influence of specular reflections in our algorithm, the measurements were still affected by this source of noise; in particular, at the edges and crests of the tooth where strong reflections are expected. Further improvements on the setup are in progress, including the addition of polarizers. Note that S_{caries} in Eq. (4) uses wavelengths below 1.7 μm. We have generated a second algorithm that performs equally well and has little influence by specular reflections; however, the algorithm requires wavelengths above 1.7 μm. A current drawback of NIR spectral imaging is the cost of the detector; CCD cameras do not work in this wavelength range, and therefore, InGaAs or MCT cameras are normally used. Note that InGaAs has a spectral response that covers up to 1700 nm, whereas MCT covers up to 2500 nm; the later being two- to threefold more expensive than the former. We have therefore developed the algorithm that could be used with an InGaAs chip.

Note that the number of teeth used in this investigation was limited by the availability, and additional tooth samples could be sourced and used in the future for further validation studies. In addition, tooth sample storage methods should ensure that its organic component (mainly collagen) is preserved. Further studies are therefore required to examine the influence of different storing methods[31] on NIR spectral imaging; however, we expect little influence since this is not a fluorescence technique where protein denaturalization could affect the signal significantly.

Although the method fails to score correctly where there is a tooth hole, this does not represent a major drawback since it can be used as an adjunct to visual inspection where this type of lesion can easily be detected.

We believe that the NIR spectral imaging method presented can be an important part of the diagnostic armament of dental practitioners and can potentially improve and simplify the decision-making process, leading to better treatment planning and to the reduction of unnecessary invasive procedures. Further *in vitro* studies to understand the relationship between this method and mineral loss by using microradiography are still needed. In addition, we believe that lesion progressions could also be followed with this method due to its quantitative nature, and this can be of great use for clinical trials; additional investigations are however required to support this capability.

References

1. A. Fejerskov, B. Nyvad, and E. A. M. Kidd, *Dental Caries The Disease and Its Clinical Management*, chap. 5, Blackwell Munksgaard, Copenhagen, Denmark (2003).
2. E. A. M. Kidd and O. Fejerskov, "What constitutes dental caries? Histopathology of carious enamel and dentin related to the action of cariogenic biofilms," *J. Dent. Res.* **83**(Spec. No. C), C35–C38 (2004).
3. C. A. Murdoch-Kinch and M. E. McLean, "Minimally invasive dentistry," *J. Am. Dent. Assoc.* **134**, 87–95 (2003).
4. K. J. Anusavice, "Present and future approaches for the control of caries," *J. Dent. Educ.* **69**, 538–554 (2005).
5. L. J. Walsh, "The current status of low level laser therapy in dentistry. Part 2. Hard tissue applications," *Aust. Dent. J.* **42**, 302–306 (1997).
6. S. H. Chin-Ying, G. Xiaoli, P. Jisheng, and J. S. Wefel, "Effects of CO2 laser on fluoride uptake in enamel," *J. Dent.* **32**, 161–167 (2004).
7. A. Wenzel, E. H. Verdonschot, G. J. Truin, and K. G. Knig, "Accuracy of visual inspection, fiber-optic transillumination, and various radiographic image modalities for the detection of occlusal caries in extracted non-cavitated teeth," *J. Dent. Res.* **71**, 1934–1937 (1992).
8. V. Machiulskiene, B. Nyvad, and V. Baelum, "A comparison of clinical and radiographic caries diagnoses in posterior teeth of 12-year-old Lithuanian children," *Caries Res.* **33**, 340–348 (1999).
9. D. F. Côrtes, K. R. Ekstrand, A. R. Elias-Boneta, and R. P. Ellwood, "An in vitro comparison of the ability of fibre-optic transillumination, visual inspection and radiographs to detect occlusal caries and evaluate lesion depth," *Caries Res.* **34**, 443–447 (2000).
10. C. Longbottom and M.-C. D. N. J. M. Huysmans, "Electrical measurements for use in caries clinical trials," *J. Dent. Res.* **83**(Spec. No. C), C76–C79 (2004).
11. R. P. Ellwood and D. F. Côrtes, "In vitro assessment of methods of applying the electrical caries monitor for the detection of occlusal caries," *Caries Res.* **38**, 45–53 (2004).
12. B. Angmar-Månsson and J. J. ten Bosch, "Optical methods for the detection and quantification of caries," *Adv. Dent. Res.* **1**, 14–20 (1987).
13. J. Brinkman, J. J. ten Bosch, and P. C. Borsboom, "Optical quantitation of natural caries in smooth surfaces of extracted teeth," *Caries Res.* **22**, 257–262 (1988).
14. A. C. Ko, M. Hewko, M. G. Sowa, C. C. Dong, B. Cleghorn, and L.-P. Choo-Smith, "Early dental caries detection using a fibre-optic coupled polarization-resolved Raman spectroscopic system," *Opt. Express* **16**, 6274–6284 (2008).
15. A. Hall and J. M. Girkin, "A review of potential new diagnostic modalities for caries lesions," *J. Dent. Res.* **83**(Spec. No. C), C89–C94 (2004).
16. C. M. Pine, in *Early Detection of Dental Caries I. Proc. of 1st Annual Indiana Conf.*, edited by G. K. Stookey, pp. 51–65, Indiana Press, Indianapolis (1996).
17. A. Schneiderman, M. Elbaum, T. Shultz, S. Keem, M. Greenebaum, and J. Driller, "Assessment of dental caries with Digital Imaging Fiber-Optic TransIllumination (DIFOTI): in vitro study," *Caries Res.* **31**, 103–110 (1997).
18. E. de Josselin de Jong, F. Sundstrm, H. Westerling, S. Tranaeus, J. J. ten Bosch, and B. Angmar-Månsson, "A new method for in vivo quantification of changes in initial enamel caries with laser fluorescence," *Caries Res.* **29**, 2–7 (1995).
19. M. H. van der Veen and E. de Josselin de Jong, "Application of quantitative light-induced fluorescence for assessing early caries lesions," *Monogr. Oral Sci.* **17**, 144–162 (2000).
20. D. Fried, R. Glena, J. Featherstone, and W. Seka, "Nature of light scattering in dental enamel and dentin at visible and near-infrared wavelengths," *Appl. Opt.* **34**, 1278–1285 (1995).
21. R. Jones and D. Fried, "Attenuation of 1310-nm 1550-nm laser light through sound dental enamel," *Lasers in Dentistry VIII*, *Proc. SPIE* **4610**, 187–190 (2002).
22. R. Jones, G. Huynh, G. Jones, and D. Fried, "Near-infrared transillumination at 1310-nm for the imaging of early dental decay," *Opt. Express* **11**, 2259–2265 (2003).
23. C. Buehler and D. Fried, "Near-IR imaging of occlusal dental decay," *Proc. SPIE* **5687**, 125–131 (2005).
24. C. Darling, G. Huynh, and D. Fried, "Light scattering properties of natural and artificially demineralized dental enamel at 1310 nm," *J. Biomed. Opt.* **11–11**, 34023 (2006).
25. D. Fried, J. Xie, S. Shafi, J. Featherstone, T. Breunig, and L. Charles,

"Imaging caries lesions and lesion progression with polarization sensitive optical coherence tomography" *J. Biomed. Opt.* **7**, 618–627 (2002).

26. G. K. Stookey, "Optical methods—quantitative light fluorescence," *J. Dent. Res.* **83**(Spec. No. C), C84–C88 (2004).

27. A. Lussi, R. Hibst, and R. Paulus, "DIAGNOdent: an optical method for caries detection," *J. Dent. Res.* **83**(Spec. No. C), C80–C83 (2004).

28. C. Lee, C. L. Darling, and D. Fried, "Polarization-sensitive optical coherence tomographic imaging of artificial demineralization on ex-posed surfaces of tooth roots," *Dent. Mater.* **25**, 721–728 (2009).

29. C. Buhler, P. Ngaotheppitak, and D. Fried, "Imaging of occlusal dental caries (decay) with near-IR light at 1310-nm," *Opt. Express* **13**, 573–582 (2005).

30. G. Jones, R. Jones, and D. Fried, "Transillumination of interproximal caries lesions with 830-nm light," *Proc. SPIE* **5313**, 17–22 (2004).

31. P. Francescut, B. Zimmerli, and A. Lussi, "Influence of different storage methods on laser fluorescence values: a two-year study," *Caries Res.* **40**, 181–185 (2006).